This is the peer-reviewed, final accepted version for American Mineralogist, published by the Mineralogical Society of America.
The published version is subject to change. Cite as Authors (Year) Title. American Mineralogist, in press.
DOI: https://doi.org/10.2138/am-2024-9414. http://www.minsocam.org/

Word count: 6082 **Revision 1**

Insights into the structure of disordered layered lead oxychlorides: Twinning and short-range order in janchevite, $Pb_9VO_{10.25}\square_{0.75}Cl_{2.5}$

GIOVANNI O. LEPORE[1,*], LUCA BINDI[1,2], FRANCESCO D'ACAPITO[3], ANNA-IRENE LANDI[1,4], PAOLA BONAZZI[1]

[1] Dipartimento di Scienze della Terra, Università di Firenze, Via La Pira 4, I-50121 Firenze, Italy
[2] C.N.R. – Istituto di Geoscienze e Georisorse, Unità di Firenze, Via G. La Pira 4, I-50121 Firenze, Italy
[3] CNR-IOM-OGG c/o ESRF – The European Synchrotron, 71 Avenue des Martyrs CS 40220, 38043 Grenoble Cédex 9, France
[4] Dipartimento di Fisica, Università di Trento, Via Sommarive 14, Povo, I-38123 Trento, Italy

*giovanniorazio.lepore@unifi.it

ABSTRACT

The crystal structure of the rare mineral janchevite was solved using intensity data collected from a twinned crystal from the Kombat mine, Namibia. This study revealed that, in spite of the strong tetragonal subcell, the structure is triclinic (space group *P*-1) with $a = 8.8382(7)$, $b = 8.8567(7)$, $c = 11.7103(17)$ Å, $\alpha = 103.385(10)$, $\beta = 94.192(10)$, $\gamma = 90.294(6)°$, $V = 889.13(16)$ Å^3, and $Z = 2$. Chemical data indicate the presence of Mo, As, and Si, besides Pb, Cl, O, and V. The refinement of an anisotropic model, which takes into account a two domains non-merohedral twinning (twinning matrix |-100/0-10/⅕⅗1|), led to an $R = 0.0522$ for 6037 independent observed reflections [$2\sigma(I)$ level] and 165 parameters and an $R = 0.0964$ for all 11701 independent reflections. The structure consists of PbO litharge sheets alternating with a layer of Cl^- anions in a 2:1 ratio. The incorporation of high-charge cations (V^{5+}, Mo^{6+}, As^{5+}, Si^{4+}) into the litharge sheet involves the formation of square cavities where

MoO_5 square pyramids and $(Si,As,V)O_4$ tetrahedra are hosted. On the basis of information gained from the chemical, structural, and spectroscopic characterization, the crystal chemical formula was revised, yielding $Pb_9VO_{10.25}\square_{0.75}Cl_{2.5}$ (Z = 2). The presence of additional apical oxygen atoms between Pb layers influences the interlayer thickness, as evident by the linear correlation between the interlayer oxygen content and the type of structural defects. A correct comprehension of short- and long-range order is crucial to understand and predict the functional properties of this family of materials.

INTRODUCTION

Layered lead oxychlorides (hereafter LLO) represent a fascinating class of materials that have garnered significant attention in the realm of solid-state chemistry and materials science (e.g. Kusainova et al. 2001; Shan et al. 2009; Salje 2015; Hirai 2024). These compounds are characterized by a structure ideally composed by litharge blocks, made of neutral layers of edge-sharing OPb_4 tetrahedra, alternated with sheets of Cl^- ions. The electroneutrality is usually reached through deviations from the ideal topology through the removal of OPb_4 groups, often associated with the insertion of anionic groups containing a number of cations such as Mo^{6+}, W^{6+}, V^{5+}, $As^{3+/5+}$, $I^{3+/5+}$, Si^{4+}, B^{3+}, Sb^{3+}, and Bi^{3+} (e.g. Siidra et al. 2008; Chukanov et al. 2019). Moreover, substitution of OH^- for O^{2-} in the PbO layer or insertion of Pb^{2+} in the chloride sheet, with the formation of square planar $PbCl_4$ groups, may occur. The resulting cavities, exhibiting different sizes and shapes, may be ordered, giving rise to several superstructures deviating from the tetragonal basic structure (*I*4/*mmm*) (e.g. Chukanov et al. 2019; Siidra et al. 2012). In many cases, the presence of superstructures has been observed by electron diffraction alone, so that scarce structural information about the incorporated groups is available (Welch et al. 1996; Welch 2004; Bindi et al. 2008).

In the context of a project aimed at improving our knowledge on the structural features of some minerals of the LLO family, we report a study focused on the mineral janchevite, ideally $Pb_7V^{5+}(O_{8.5}\square_{0.5})Cl_2$ (Chukanov et al. 2018), an oxygen-deficient, V-analogue of parkinsonite, ideally $Pb_7MoO_9Cl_2$ (Symes et al. 1994; Lepore and Welch 2010).

According to Chukanov et al. (2018), the tetragonal average janchevite structure can be described as a 2:1 alternation of Pb–O blocks and sheets of Cl^- ions. V and other substituent cations (Mo and minor amounts of Si) are supposed to randomly replace Pb in the litharge block.

In order to investigate the crystal-chemical environment of V, Mo and other substituents and their possible ordering schemes in the structure of janchevite, a chemical, structural and spectroscopic study was undertaken on a sample from the type-locality, Kombat mine, Namibia (sample 3740/I, Museo di Storia Naturale, Università di Firenze, Italy). The results are presented here.

EXPERIMENTAL METHODS

Electron probe microanalysis. Four janchevite crystals were embedded in epoxy resin, polished with diamond paste down to 0.25 μm and then coated with a ~28 nm-thick graphite layer. Chemical analysis was carried out using a JEOL-JXA-8230 electron microprobe operated at 15 kV and 10 nA and 5 μm beam diameter. The calibration standards used were crocoite (for Pb-*M*α), tugtupite (for Cl-*K*α), GaAs (for As-*L*α), Mo and V metal (for Mo-*L*α and V-*K*α, respectively) and albite (for Si-*K*α). The data were corrected for matrix effects using the ΦρZ method of the JEOL software package. The average composition (means and ranges in wt.% of oxides) is reported in Table 1.

Single-crystal X-ray diffraction. A fragment of about 0.05×0.03×0.01 mm^3 was selected and examined by means of a Bruker D8 Venture single-crystal X-ray diffractometer operated at 50 kV and 40 mA and equipped with a Photon 100 CMOS detector system, employing graphite-monochromatized

This is the peer-reviewed, final accepted version for American Mineralogist, published by the Mineralogical Society of America.
The published version is subject to change. Cite as Authors (Year) Title. American Mineralogist, in press.
DOI: https://doi.org/10.2138/am-2024-9414. http://www.minsocam.org/

Mo*K*α radiation (λ = 0.71073 Å). Indexing of reflections led to the triclinic unit cell with a = 8.8382(7), b = 8.8567(7), c = 11.7103(17) Å, α = 103.385(10), β = 94.192(10), γ = 90.294(6)°, and V = 889.13(16) Å^3. Many other crystals were also tested, all leading to similar unit-cell values. The strongest reflections are consistent with the tetragonal I subcell [a = 3.9542(1) c =22.708(1) Å] previously reported for janchevite. Intensity integration and standard Lorentz-polarization corrections were performed with the *CrysAlis* RED (CrysAlisPRO 2014) software package. The program ABSPACK in *CrysAlis* RED was used for the absorption correction. A full sphere (up to sinθ/λ ~ 0.75) was collected, yielding 11701 independent reflections in the -1 Laue group. A careful examination of the collected intensity data revealed the coexistence of two twin domains related by the twinning matrix |-100/0-10/⅕⅗⅕1|. Data reduction was then carried out accordingly (R_{int} = 0.080 for reflections from both twin domains). The structure solution was carried out in the P-1 space group using direct methods (Sheldrick 2008). Ten heavy atoms (Pb1-to-Pb10) were identified in the Fourier map and initially refined as Pb *vs.* structural vacancy. Pb1-Pb9 were fully occupied by Pb and their occupancy was fixed accordingly. Refined electron density of Pb10 was lower and the site was observed to be split into two partially occupied positions (M10a and M10b). M10b was considered occupied by the minor amount of metals substituting for Pb (V, Mo, As and Si) and refined using the Mo scattering curve. The resulting electron density at the site is in agreement with the weighted mean electron number of the above elements in the proportion obtained from EPMA data (Table 1). In the subsequent cycles, three peaks were assigned to Cl. Eleven oxygen atoms were then located in the difference Fourier map and their occupancy was initially left free to vary. O1-O6 were fully occupied by O while O7-O11 showed a partial occupancy. Noteworthy, atoms O7-O10, close to Ma10a-M10b, showed extremely large atomic displacement parameters (ADPs). So, we decided to fix their ADPs to 0.05 Å^2 and keep free their occupancies free to refine. At the last stage, all atom positions, apart O atoms, were refined anisotropically up to the residual value R = 0.0522 for 6037 independent observed reflections [2σ(I)

level] and 165 parameters and at $R = 0.0964$ for all 11701 independent reflections. Neutral scattering curves were taken from the International Tables of Crystallography (Wilson 1992). Selected interatomic distances and site scattering (s.s.) values are shown in Table 2. Details relating to data collection and structure refinement, atomic coordinates and displacement parameters are available in the CIF file deposited at the editorial office of The American Mineralogist.

X-ray Absorption Spectroscopy (XAS). Several crystals, sufficient to keep the total absorption coefficient $\mu \leq 1.5$ at all the measured edges, were hand-picked, powdered, and pressed in a 3 mm pellet with cellulose. XAS measurements were performed at the "LISA" CRG beamline (BM-08) (d'Acapito et al. 2019) at the European Synchrotron Radiation Facility (ESRF, Grenoble, France) at the *K*-edges of V, As, and Mo (5465.1, 11866.7 and 19999.5 eV, respectively). Measurements were performed using a pair of Si (111) (for V and As *K* edges) and Si (311) (for Mo *K* edge) flat monochromator crystals. Si- and Pt-coated focusing mirrors ($E_{\text{cut-off}} \approx 16$ and 40 keV, respectively) were used for harmonic rejection, providing a beam of a roughly circular spot with a diameter of ≈ 200 μm. The step size in the XANES (X-ray absorption near-edge structure) region was 0.3 eV for V and As *K*-edge measurements and 0.5 eV for Mo *K*-edge; the pre-edge region of V *K*-edge was sampled with 0.2 eV steps. The post-edge EXAFS (extended X-ray absorption fine structure) region of the spectrum was acquired with a fixed k step width of 0.05 $Å^{-1}$. Measurements were performed in fluorescence mode by means of a 12-element solid state (high purity germanium) detector (Puri et al. 2019). The following model compounds were also measured in the transmission mode: vanadinite [$(Pb_5(VO_4)_3Cl$] and cavansite [$Ca(VO)Si_4O_{10}•4(H_2O)$](Giuli et al. 2004; Moretti et al. 2013), V_2O_5, V_2O_3, adamite [$Zn_2(AsO_4)(OH)$] (George et al. 2019), As_2O_5, As_2O_3, MoO_3, MoO_2. All measurements were carried out at room temperature. Standard procedures (Lee et al. 1981) were followed to extract the structural EXAFS signal ($k•\chi(k)$): pre-edge background removal, spline modelling of bare atomic background, edge step normalization using a far above the edge region, and energy calibration using

the software ATHENA (Ravel and Newville 2005). Model atomic clusters centered on the absorber atom were obtained by ATOMS (Ravel 2001); theoretical amplitude and phase functions were generated using the FEFF8 code (Ankudinov et al. 1998) starting from the structural model presented in this study. EXAFS spectra were fitted through the ARTEMIS software (Ravel and Newville 2005) in the Fourier-Transform (FT) space.

RESULTS AND DISCUSSION

Chemical composition

The chemical composition of the studied sample is very close to that reported by Chukanov et al. (2018) although it also contains significative amounts of As, besides V, Mo and Si. On the basis of XAS data we can infer information on oxidation states of the cations substituting for Pb. Vanadium *K*-edge in janchevite lies at the same position as in V_2O_5 and vanadinite (Fig. 1a and b) indicating it occurs as V^{5+}; the same applies to As *K*-edge (Fig. 1c), lying at the same energy value observed for adamite and As_2O_5, pointing to the presence of As^{5+} only. The comparison between the Mo *K*-edge spectrum in janchevite and those of MoO_2 and MoO_3 indicates that Mo in janchevite is hexavalent (Fig. 1d). Taking into account all the observations, the empirical formula of janchevite was calculated on $\Sigma_{(Pb+V+Mo+As+Si)} = 10$ *apfu* yielding the formula $Pb_{9.09}V_{0.30}Mo_{0.33}As_{0.15}Si_{0.13}O_{10.16}Cl_{2.61}$ (Table 1). The overall mean electron number (27.53) is in excellent agreement with that derived from the structural refinement (27.30; Table 2).

Twinning and superstructure

The investigated crystal was made of two twin domains (I and II in the proportion 52:48) with domain I related to domain II by the twinning matrix |-100/0-10/⅕¾⅕1|. There are three different categories of reflections (Figure 2): the first one from domain I only (blue), the second one from domain II only

(red), and the third one grouping the overlapped reflections. The condition for reflection overlapping is $h + 3k = 5n$, corresponding to the subcell reflections. In Figures 2a and 2b are reported the twinned *h*0*l* and 0*kl* planes showing the additional binary symmetry introduced by twinning; the [001] twin axis in the direct space is shown in Figure 2c. The pattern observed in Figure 2d, where the (*hk*0) reconstruction is shown, is very similar to what was observed by Welch et al. (1996) in the electron diffraction pattern of a V-rich parkinsonite. Welch et al. (1996) also observed the occurrence of a monoclinic distortion in some of the superstructure reflection quartets of the pattern, which was attributed to the presence of V. The triclinic *P* unit cell found here for janchevite is related to the tetragonal *I* subcell by the transformation matrix |⅖⅕0/-⅕⅖0/⅕⅗2|; the *hk*0 plane of the *P* unit cell is thus not coplanar with that of the *I* unit cell. In light of this result, a further thing to take into account in the analysis of the distortion in the SAED pattern of V-rich parkinsonite is the possibility that, as in janchevite, the *hk*0 plane of the superstructure observed by Welch et al. (1996) is not coplanar with the *hk*0 plane of the substructure thus likely affecting the geometry of the observed pattern.

Crystal structure and short-range order

Analogously to other minerals within the family of layered lead oxychlorides, janchevite shows a structural arrangement consisting of PbO litharge sheets alternating with square-net layers of Cl-anions. In particular, as already argued by Chukanov et al. (2018), the stacking sequence exhibits a PbO:Cl ratio of 2:1 (Fig.3). However, the incorporation of high-charge cations replacing Pb in the litharge sheet is not completely disordered as originally supposed but gives rise to a superstructure. The ordering scheme that results in such a superstructure can be readily visualized by employing an oxocentered representation of the PbO sheet made of OPb_4 units (Fig. 4a). Compared to an ideal litharge structure, O7, O8, O9, and O10, which showed large ADPs, are partially occupied and displaced from the ideal center of the OPb_3M tetrahedron towards M10b. Accordingly, high-charge M cations are bonded to 4 oxygen atoms and to a further, partially occupied, apical oxygen (O11). This arrangement results in a

square pyramidal geometry with 4 longer basal bonds (~1.83 Å) and one shorter apical bond (~1.71 Å). Bond-valence sums for cations and anions in the refined model are listed in Table 3. They are in general agreement with the expected oxidation states. The low sum on most of the oxygen atoms forming the square pyramid can be ascribed to the intrinsic difficulty in accurately characterizing the disordered MO_5 polyhedron. Following the topological description proposed by Siidra et al. (2008) and Chukanov et al. (2019), janchevite can thus be seen as characterized by square DN4 cavities (Fig. 4b), DN standings for defect number, where a square-pyramidal (MO_5) group substitutes four OPb_4 units. However, although the coordination of cations such as V^{5+}, Mo^{6+}, $Si^{4+}$and As^{5+} may vary significantly, this kind of bonding geometry is extremely unlikely in the case of Si and As. The actual geometry of each M polyhedron remains thus indistinct in the average structure. Additional details on this aspect have been obtained by the XAS results, which indicate a distinct environment for Mo^{6+} on one side and As^{5+} and V^{5+} on the other; Si coordination, despite the lack of XAS data, can be statistically safely assumed as tetrahedral (Waroquiers et al. 2017). The comparison of XANES data at V *K*-edge with model compounds (Fig. 1a) clearly indicates that the V local environment in janchevite is extremely close to that of vanadinite, thus occurring as VO_4^{3-} groups as in kombatite (Cooper and Hawthorne 1994), hereroite (Turner et al. 2012) and erikjonssonite (Chukanov et al. 2019). The same goes for As: As *K*-edge XANES (Fig. 1b) shows a marked similarity of janchevite spectrum with that of adamite, where As^{5+} is in the typical tetrahedral coordination as in sahlinite (Bonaccorsi and Pasero 2003). In line with this, the EXAFS fit (Fig. 5a, Table 4) yields an As-O mean bond length of 1.69 Å with four oxygen atoms thus in line with what observed in sahlinite (<As-O> = 1.694 Å). In the case of Mo, the XANES spectrum (Fig. 1c) suggests that Mo in janchevite is hosted within a strongly distorted, non-centrosymmetric coordination such as tetrahedral or pentahedral, as evidenced by the pronounced intensity of the pre-edge peak compared to that of the nonetheless distorted, octahedrally-coordinated Mo in molybdenite. Mo XANES in janchevite closely resembles the case of parkinsonite, the Mo

analogue of janchevite, described in detail by Welch et al. (1996) where the intensity of the pre-edge peak was attributed to Mo^{6+} in pentahedral coordination. This interpretation is quantitatively confirmed for janchevite by the results of the EXAFS fit (Fig. 5b, Table 4) that indicates a 4+1 geometry with four 1.88 and one 1.74 Å Mo-O distances for the first coordination shell of Mo, yielding a bond-valence sum on Mo of ~5.9 v.u.. The analysis of the second coordination shell around Mo is in substantial agreement with the average model. The local coordination of Si, V and As in janchevite is thus in disagreement with the average structure, which implies mainly a [4+1] bonding geometry for M cations. However, the partial occupancy of the 4 basal oxygens, together with their high displacement parameters, indicates a significant level of positional disorder. This is likely the effect of the disordered distribution of MoO_5 square pyramids and $(Si,As,V)O_4$ tetrahedral groups in different orientations within the DN4 cavity. The presence of additional oxygen atoms in between Pb layers, which are normally connected by lone-pair interactions only, causes a strengthening of the interlayer bonding (note the long O11-Pb distances in Table 2), yielding a contraction of the interlayer thickness. The extent of the contraction is indeed linearly correlated with the number of apical oxygens in the interlayer as can be seen from Figure 6, where the ratio between apical oxygens and the interlayer thickness (IT) of adjacent Pb layers is plotted. LLO with 2:1 (PbO:Cl) ratio basically divide into 3 groups, showing an excellent trend between the amount of additional oxygens between Pb layers and, consequently, the number and type of defects in the PbO layer and the IT. Hence, phases like sahlinite (Bonaccorsi and Pasero 2003) and kombatite (Cooper and Hawthorne 1994), with a PbO layer characterized by double square (DN7) cavities where tetrahedral groups are hosted, show the shortest IT among the 2:1 LLO, while janchevite, having DN4 cavities and thus a lower density of interlayer oxygen atoms, has the largest one. Hereroite (Siidra et al. 2013) and erikjonssonite (Chukanov et al. 2019), having both DN4 and DN7 cavities, show intermediate values. The equation, IT (Å) = 2.648 – $0.711(O_{apical}/Pb)$, can also be used to hypothesize the type of cavities in phases like asisite and

parkinsonite, where such information has not been determined yet, on the basis of the *z* coordinate of the Pb2 site in the *I*4/*mmm* substructure; as a matter of fact, both minerals fall in the field of DN4 cavities, suggesting a strong similarity with janchevite (Fig. 6). This is not surprising for parkinsonite, given the analogies with janchevite highlighted by the comparison between this study and TEM data (Welch et al. 1996). In the case of asisite, Welch (2004) suggested a $Pb_{12}Si$ superstructure on the basis of TEM observations which would not be compatible with the superstructure of janchevite and parkinsonite; however Welch (2004) also pointed out that different chemical compositions can occur for asisite (e.g., Rouse et al. 1988) and this could produce distinct superstructures arising from slightly different Pb-Si ordering.

Nomenclature remarks

From a chemical point of view, janchevite is close to erikjonssonite, where V, Mo, As and Si polyhedra are hosted in two different types of cavities. The substitution scheme in janchevite is apparently more disordered, yielding to the formation of DN4 cavities only, as in the 1:1 LLO symesite (Welch et al. 2000). The DN4 sheet has $[Pb_9O_6]^{6+}$ stoichiometry yielding, taking into account 2.5 Cl^- atoms, a negative charge deficit of 3.5, which is balanced by the incorporation of square-pyramidal (MO_5) anionic groups. The integrated analysis of single-crystal X-ray diffraction and EXAFS data provides a deeper look on the origin of the disorder related to the substitution of Pb by other elements. XAS results indicate an ordered local environment for Mo, As and V, each having a distinct coordination which deviates from the average structure. The complex structure of janchevite then arises from the combination of two types of partially ordered substitution mechanisms, one related to the formation of the DN4 cavities and their stacking sequence, and the other to the distribution of tetrahedral and square-pyramidal groups inside the cavities. These observations, along with what previously reported for parkinsonite and asisite (Welch et al. 1996; Welch 2004; Lepore and Welch 2010), raise the question as to whether defect-free (DN0) structures (e.g. Rouse and Dunn 1985; Welch et al. 2001)

238 actually exist when Pb atoms are substituted by very different elements in both size and charge. The
239 difficulty in defining the actual structure of some LLO minerals has important nomenclature
240 implications, since the lack of a structural formula, as already emphasized (Welch et al. 1996; Welch
241 2004; Lepore and Welch 2010), may lead to inaccurate classification. In the case of janchevite, the
242 ideal stoichiometry proposed by Chukanov et al. (2018) should be revised to $Pb_9VO_{10.25}\square_{0.75}Cl_{2.5}$. Such
243 a formula would imply a 5-fold coordination of part of V atoms (0.25 apfu) which has never been
244 reported in members of the LLO family. It is then possible that this constraint prevents the formation of
245 pure V end-members. The Pb_9V stoichiometry also agrees with the $Pb_9MoO_{11}Cl_2$ formula proposed by
246 Welch et al. (1996) and Lepore and Welch (2010) for parkinsonite based on TEM and EPMA
247 observations. This similarity allows us to define a general formula for the janchevite-parkinsonite join
248 as $Pb_9V_{1-x}Mo_xO_{(10.25+3/4x)}Cl_{2.5-x/2}$, where the V/Mo ratio dictates the number of oxygens in the cavities
249 and the Cl deficiency.
250

251 ## IMPLICATIONS

252 The solution of the crystal structure of janchevite offers the opportunity to make some general
253 comments on the importance of deciphering fine structural details in disordered layered lead
254 oxychlorides. It indeed provides insights into the relationship between atomic structure and physical
255 and chemical properties, which is crucial for tailoring materials with specific functionalities, such as
256 electronic, magnetic, optical, or catalytic properties. In this light, the investigation of short-range
257 ordering phenomena is even more important, since they are often reported to have a strong impact on
258 several properties of functional materials (e.g. Keen and Goodwin 2015). Furthermore, the knowledge
259 gained from studying these compounds can guide the design and synthesis of new materials with
260 enhanced properties as those for applications ranging from energy storage and conversion to sensing
261 and environmental remediation. Layered oxychloride heteroanionic compounds have, for example,

recently emerged as materials with unique electronic properties, having potential optical and quantum magnetic applications (Harada et al. 2019; Hirai 2024). Moreover, layered oxychlorides are promising candidates for rechargeable battery electrodes due to their unique structural characteristics (Gao et al. 2016). Thus, understanding the relationship between short- and long-range order in these materials and its impact on their chemical and physical properties can lead to the development of high-performance and stable battery systems for energy storage applications, including electric vehicles and grid storage.

Acknowledgements

This paper is dedicated to the memory of Paola Bonazzi, who recently and prematurely passed away. Her passing left us stunned and bereft of a mentor. Paola was a teacher to many of us and aided and supported us throughout our academic and human progress. Her influence left an indelible mark on all who had the privilege to learn from her. She will be deeply missed.

G.O.L. is grateful to Mark D. Welch for introducing him, now many years ago, to the intriguing family of layered lead oxychlorides. The authors would like to thank Massimo Batoni for donating the janchevite sample to the Museo di Storia Naturale. The manuscript benefited from the helpful review of Sergey V. Krivovichev and an anonymous reviewer. This work has been funded by The Italian Society of Mineralogy and Petrology (SIMP) through the Research Grant in memory of Prof. Fiorenzo Mazzi awarded to G.O.L. The CERIC-ERIC Consortium is acknowledged for the access to LISA beamline at ESRF [Proposal no. 20212113/A08-01-1079 (CERIC-ERIC/ESRF) “Short-range order in layered lead oxychlorides]. X-ray intensity data were collected at CRIST, Centro di Cristallografia Strutturale, University of Florence, Italy. EPMA data were collected at LaMA - Laboratorio di MicroAnalisi, University of Florence/CNR-IGG.

References

Ankudinov, A.L., Ravel, B., Rehr, J.J., and Conradson, S.D. (1998) Real-space multiple-scattering calculation and interpretation of x-ray-absorption near-edge structure. Physical Review B, 58, 7565.

Bindi, L., Welch, M.D., Bonazzi, P., Pratesi, G., and Menchetti, S. (2008) The crystal structure of seeligerite, $Pb_3IO_4Cl_3$, a rare Pb-I-oxychloride from the San Rafael mine, Sierra Gorda, Chile. Mineralogical Magazine, 72, 771–783.

Bonaccorsi, E., and Pasero, M. (2003) Crystal structure refinement of sahlinite $Pb_{14}(AsO_4)_2O_9Cl_4$. Mineralogical Magazine, 67, 15–21.

Brese, N.E., and O'Keeffe, M. (1991) Bond-valence parameters for solids. Acta Crystallographica Section B: Structural Science, 47, 192–197.

Chukanov, N.V., Nekrasova, D.O., Siidra, O.I., Polekhovsky, Y.S., and Pekov, I.V. (2018) Janchevite, $Pb_7V^{5+}(O_{8.5}\square_{0.5})Cl_2$, A New Mineral From the Kombat Mine, Namibia. The Canadian Mineralogist, 56, 159–165.

Chukanov, N.V., Siidra, O.I., Polekhovsky, Y.S., Pekov, I.V., Varlamov, D.A., Ermolaeva, V.N., and Virus, A.A. (2019) Erikjonssonite, $(Pb_{32}O_{21})[(V,Si,Mo,As)O_4]_4Cl_9$, a new mineral from the Kombat mine and structural classification of layered lead oxychlorides related to litharge. European Journal of Mineralogy, 31, 619–628.

Cooper and Hawthorne (1994) The crystal structure of kombatite, $Pb_{14}(VO_4)_2O_9Cl_4$, a complex heteropolyhedral sheet mineral.

CrysAlisPRO, O.D. (2014) Agilent Technologies UK Ltd. Yarnton, England, 1.

306 d'Acapito, F., Lepore, G.O., Puri, A., Laloni, A., La Manna, F., Dettona, E., De Luisa, A., and Martin,
307 A. (2019) The LISA beamline at ESRF. Journal of synchrotron radiation, 26, 551–558.

308 Gagné, O.C., and Hawthorne, F.C. (2015) Comprehensive derivation of bond-valence parameters for
309 ion pairs involving oxygen. Acta Crystallographica Section B: Structural Science, Crystal
310 Engineering and Materials, 71, 562–578.

311 Gao, P., Lin, X.M., Reddy, M.A., Zhang, L., Diemant, T., Behm, R.J., and Fichtner, M. (2016)
312 Electrochemical Behavior of Layered Vanadium Oxychloride in Rechargeable Lithium Ion
313 Batteries. Journal of The Electrochemical Society, 163, A2326–A2332.

314 George, L.L., Biagioni, C., Lepore, G.O., Lacalamita, M., Agrosì, G., Capitani, G.C., Bonaccorsi, E.,
315 and d'Acapito, F. (2019) The speciation of thallium in (Tl, Sb, As)-rich pyrite. Ore Geology
316 Reviews, 107, 364–380.

317 Giuli, G., Paris, E., Mungall, J., Romano, C., and Dingwell, D. (2004) V oxidation state and
318 coordination number in silicate glasses by XAS. American Mineralogist, 89, 1640–1646.

319 Harada, J.K., Charles, N., Poeppelmeier, K.R., and Rondinelli, J.M. (2019) Heteroanionic Materials by
320 Design: Progress Toward Targeted Properties. Advanced Materials, 31, 1805295.

321 Hirai, D. (2024) Pinalites: Optical Properties and Quantum Magnetism of Heteroanionic $A_3MO_5X_2$
322 Compounds. Inorganic Chemistry, 63, 4001–4010.

323 Keen, D.A., and Goodwin, A.L. (2015) The crystallography of correlated disorder. Nature, 521, 303–
324 309.

325 Krivovichev, S.V. (2012) Derivation of bond-valence parameters for some cation-oxygen pairs on the
326 basis of empirical relationships between r_0 and b. Zeitschrift für Kristallographie - Crystalline
327 Materials, 227, 575–579.

328 Kusainova, A.M., Lightfoot, P., Zhou, W., Stefanovich, S.Yu., Mosunov, A.V., and Dolgikh, V.A.
329 (2001) Ferroelectric Properties and Crystal Structure of the Layered Intergrowth Phase
330 $Bi_3Pb_2Nb_2O_{11}Cl$. Chemistry of Materials, 13, 4731–4737.

331 Lee, P.A., Citrin, P.H., Eisenberger, P. T, and Kincaid, B.M. (1981) Extended x-ray absorption fine
332 structure—its strengths and limitations as a structural tool. Reviews of Modern Physics, 53, 769.

333 Lepore, G.O., and Welch, M.D. (2010) The crystal structure of parkinsonite, nominally $Pb_7MoO_9Cl_2$: a
334 naturally occurring Aurivillius phase. Mineralogical Magazine, 74, 269–275.

335 Moretti, A., Giuli, G., Nobili, F., Trapananti, A., Aquilanti, G., Tossici, R., and Marassi, R. (2013)
336 Structural and electrochemical characterization of vanadium-doped $LiFePO_4$ cathodes for
337 lithium-ion batteries. Journal of the electrochemical society, 160, A940.

338 Puri, A., Lepore, G.O., and d'Acapito, F. (2019) The new beamline LISA at ESRF: performances and
339 perspectives for earth and environmental sciences. Condensed Matter, 4, 12.

340 Ravel, B. (2001) ATOMS: crystallography for the X-ray absorption spectroscopist. Journal of
341 synchrotron radiation, 8, 314–316.

342 Ravel, B., and Newville, M. (2005) ATHENA, ARTEMIS, HEPHAESTUS: data analysis for X-ray
343 absorption spectroscopy using IFEFFIT. Journal of synchrotron radiation, 12, 537–541.

344 Rouse, R.C., Peacor, D.R., Dunn, P.J., Criddle, A.J., Stanley, C.J., and Innes, J. (1988) Asisite, a
345 silicon-bearing lead oxychloride from the Kombat mine, South West Africa (Namibia). American
346 Mineralogist, 73, 643-650.

347 Rouse, R.C., and Dunn, P.J. (1985) The structure of thorikosite, a naturally occurring member of the
348 bismuth oxyhalide group. Journal of Solid State Chemistry, 57, 389–395.

Salje, E.K.H. (2015) Modulated minerals as potential ferroic materials. Journal of Physics: Condensed Matter, 27, 305901.

Shan, Z., Lin, X., Liu, M., Ding, H., and Huang, F. (2009) A Bi-based oxychloride $PbBiO_2Cl$ as a novel efficient photocatalyst. Solid State Sciences, 11, 1163–1169.

Sheldrick, G.M. (2008) A short history of SHELX. Acta Crystallographica Section A: Foundations of Crystallography, 64, 112–122.

Siidra, O. I., Krivovichev, S. V., Turner, R. W., Rumsey, M. S., and Spratt, J. (2013) Crystal chemistry of layered Pb oxychloride minerals with PbO-related structures: Part I. Crystal structure of hereroite,$[Pb_{32}O_{20}(O,\square)](AsO_4)_2[(Si,As,V,Mo)O_4]_2Cl_{10}$. American Mineralogist, 98, 248-255.

Siidra, O.I., Krivovichev, S.V., and Filatov, S.K. (2008) Minerals and synthetic Pb(II) compounds with oxocentered tetrahedra: review and classification. Zeitschrift für Kristallographie - Crystalline Materials, 223, 114–125.

Siidra, O.I., Krivovichev, S.V., Turner, R.W., and Rumsey, M.S. (2012) Natural and synthetic layered Pb (II) oxyhalides. Minerals as advanced materials II, 319–332.

Symes, R.F., Cressey, G., Griddle, A.J., Stanley, C.J., Francis, J.G., & Jones, G.C. (1994). Parkinsonite,$(Pb, Mo, \square)_8O_8Cl_2$, a new mineral from Merehead Quarry, Somerset. Mineralogical Magazine, 58, 59-68.

Turner, R., Siidra, O.I., Rumsey, M.S., Krivovichev, S.V., Stanley, C.J., and Spratt, J. (2012) Hereroite and vladkrivovichevite: two novel lead oxychlorides from the Kombat mine, Namibia. Mineralogical Magazine, 76, 883–890.

Waroquiers, D., Gonze, X., Rignanese, G.M., Welker-Nieuwoudt, C., Rosowski, F., Göbel, M., Schenk, S., Degelmann, P., André, R., Glaum, R., and others (2017) Statistical Analysis of Coordination Environments in Oxides. Chemistry of Materials, 29, 8346–8360.

Welch, M.D. (2004) Pb-Si ordering in sheet-oxychloride minerals: the super-structure of asisite, nominally $Pb_7SiO_8Cl_2$. Mineralogical Magazine, 68, 247–254.

Welch, M.D., Schofield, P.F., Cressey, G., and Stanley, C.J. (1996) Cation ordering in lead-molybdenum-vanadium oxychlorides. American Mineralogist, 81, 1350–1359.

Welch, M.D., Cooper, M.A., Hawthorne, F.C., and Criddle, A.J. (2000) Symesite, $Pb_{10}(SO_4)O_7Cl_4(H_2O)$, a new PbO-related sheet mineral: Description and crystal structure. American Mineralogist, 85, 1526–1533.

Welch, M.D., Hawthorne, F.C., Cooper, M.A., and Kyser, T.K. (2001) Trivalent Iodine in the Crystal Structure of Schwartzembergite, $Pb^{2+}_5I^{3+}O_6H_2Cl_3$. The Canadian Mineralogist, 39, 785–795.

Wilson, A.J.C. (1992) International Tables for Crystallography, vol. C, Tables 6.1. 1.4 (pp. 500–502), 4.2. 6.8 (pp. 219–222), and 4.2. 4.2 (pp. 193–199). Kluwer Academic Publishers, Dordrecht.

Figure Captions

Figure 1. Normalized XANES spectra of janchevite and selected model compounds: a) V K-edge with b) detailed comparison between vanadinite and janchevite; c) As-K edge; d) Mo-K edge. Given the small difference in energy position between Mo^{4+} and Mo^{6+}, vertical lines in d) have been added indicating the position of the main inflection point, which, by convention, is considered to be the absorption edge energy. Mo^{4+} in MoO_2 has the absorption edge at 20014 eV while MoO_3 and janchevite have absorption edge at 20016 eV.

This is the peer-reviewed, final accepted version for American Mineralogist, published by the Mineralogical Society of America.
The published version is subject to change. Cite as Authors (Year) Title. American Mineralogist, in press.
DOI: https://doi.org/10.2138/am-2024-9414. http://www.minsocam.org/

391 **Figure 2.** Reconstructed precession images showing the *h*0*l* (a), 0*kl* (b) and *hk*0 (d) planes. The
392 superstructure scheme in black in (d) is taken from (Welch et al. 1996). In (c), the [001] twin axis
393 in the direct space is shown along with a representation of the two unit-cells.

394 **Figure 3.** The crystal structure of janchevite based on oxocentered tetrahedra as seen down [100]. OPb_4
395 tetrahedra in red, Cl atoms in green, MO_5 groups in orange.

396 **Figure 4.** Projection down [001] of the PbO sheet in litharge (a) and janchevite (b) with MO_5
397 polyhedra (in orange) filling DN4 cavities (highlighted in green).

398 **Figure 5.** a) As- and b) Mo K-edge EXAFS of janchevite. Black lines are data, and red lines are fits.

399 **Figure 6.** Thickness variation of the Cl free interlayer sheet between litharge units as a function of the
400 relative abundance of oxygen atoms in the interlayer. The Oapical/Pb ratio for parkinsonite and
401 asisite was calculated on the basis of the formulae proposed by Welch et al. (1996) and Welch
402 (2004), respectively.

403

404

405 **Table 1.** Chemical composition (in wt% of oxides) of janchevite

	Mean	Ranges	S.D.
PbO	90.92	90.11-92.12	0.60
As_2O_5	0.80	0.63-1.04	0.13
MoO_3	2.15	1.88-2.51	0.21
V_2O_5	1.21	0.99-1.41	0.14
SiO_2	0.34	0.30-0.40	0.03
Cl	4.14	3.99-4.27	0.10
O_{eq}	0.93		
Total	98.63		

406

407

408

409

410

411

412 **Table 2** Selected bond distances and site scattering (*s.s.*) values

Pb1—O5	2.41 (1)	Pb4—O3	2.29 (1)	Pb7—O1	2.25 (1)
Pb1—O2^{i}	2.42 (1)	Pb4—O1	2.29 (1)	Pb7—O5	2.29 (1)
Pb1—O1^{ii}	2.43 (1)	Pb4—O9	2.59 (2)	Pb7—O6	2.38 (1)
Pb1—O4	2.45 (1)	Pb4—O7	2.64 (2)	Pb7—O7	2.60 (2)
<Pb1—O>	2.43	<Pb4—O>		Pb7—O11	2.92 (2)
Pb1—Cl1	3.358 (1)	Pb3—Cl2	3.365 (4)	<Pb7—O>	2.49
Pb1—Cl2	3.340 (5)	Pb3—Cl2’	3.434 (4)	*s.s.*	82.00
Pb1—Cl2’	3.414 (5)	Pb3—Cl3	3.140 (6)		
Pb1—Cl3	3.279 (6)	Pb3—Cl3’	3.494 (6)	Pb8—O2	2.19 (1)
<Pb1—Cl>	3.348	<Pb4—Cl>	3.358	Pb8—O4	2.30 (1)
s.s.	82.00	*s.s.*	82.00	Pb8—O6	2.37 (1)
				Pb8—O10	2.64 (2)
Pb2—O3	2.30 (1)	Pb5—O4	2.28 (1)	Pb8—O11	2.97 (2)
Pb2—O2	2.35 (1)	Pb5—O6^{ii}	2.30 (1)	<Pb8—O>	2.49
Pb2—O8	2.39 (2)	Pb5—O7	2.47 (1)	*s.s.*	82.00
Pb2—O10	2.66 (2)	Pb5—O8	2.74 (1)		
<Pb2—O>	2.423	<Pb5—O>	2.44	Pb9—O5	2.26 (1)
Pb2—Cl1	3.372 (1)	Pb5—Cl1	3.301 (1)	Pb9—O2	2.31 (1)
Pb2—Cl2	3.276 (5)	Pb5—Cl2	3.329 (5)	Pb9—O3	2.33 (1)
Pb2—Cl3	3.242 (4)	Pb5—Cl3	3.306 (5)	Pb9—O9	2.63 (2)
Pb2—Cl3’	3.581 (6)	Pb5—Cl3	3.519 (7)	Pb9—O11	3.01 (2)
<Pb2—Cl>	3.368	<Pb5—Cl>	3.364	<Pb9—O>	2.508
s.s.	82.00	*s.s.*	82.00	*s.s.*	82.00
Pb3—O6	2.31 (1)	Pb6—O4	2.22 (1)	M10a—O7	1.85 (2)
Pb3—O5	2.31 (1)	Pb6—O1^{ii}	2.28 (1)	M10a—O8	2.04 (2)
Pb3—O10	2.47 (2)	Pb6—O3	2.41 (1)	M10a—O9	2.04 (2)
Pb3—O9	2.55 (2)	Pb6—O8	2.62 (2)	M10a—O10	2.22 (3)
<Pb3—O>	2.41	Pb6—O11	2.92 (2)	<M10a—O>	2.04
Pb3—Cl1	3.382(1)	<Pb6—O>	2.49	*s.s.*	10.82
Pb3—Cl2	3.387(4)	*s.s.*	82.00		
Pb3—Cl2	3.269(4)			M10b—O11	1.71 (2)

Pb3—Cl3	3.515(6)	M10b—O8	1.82 (2)
<Pb3—Cl>	3.388	M10b—O10	1.82 (2)
s.s.	82.00	M10b—O9	1.82 (2)
		M10b—O7	1.87 (2)
		<M10b—O>	1.81
		s.s.	27.30

Table 3 Bond-valence values for janchevite

	Pb1	**Pb2**	**Pb3**	**Pb4**	**Pb5**	**Pb6**	**Pb7**	**Pb8**	**Pb9**	**M10a**	**M10b***	**Sum**	***Theor.***
O1	0.38			0.51		0.53	0.56					**1.98**	*2.00*
O2	0.40	0.46						0.63	0.49			**1.98**	*2.00*
O3		0.51		0.51		0.41			0.48			**1.91**	*2.00*
O4	0.37				0.52	0.59		0.51				**1.99**	*2.00*
O5	0.40		0.50				0.51		0.55			**1.96**	*2.00*
O6			0.50		0.51		0.43	0.43				**1.87**	*2.00*
O7 (89%)				0.22	0.32		0.28			0.15	0.78	**1.75**	*1.78*
O8 (87%)		0.37			0.18	0.23				0.10	0.72	**1.60**	*1.74*
O9 (74%)			0.22	0.21					0.19	0.08	0.61	**1.31**	*1.48*
O10 (72%)		0.17	0.26					0.18		0.06	0.60	**1.27**	*1.44*
O11 (87%)						0.13	0.13	0.13	0.10		0.95	**1.44**	*1.74*
Cl1	$0.11^{\times 2\rightarrow}$	$0.10^{\times 2\rightarrow}$	$0.09^{\times 2\rightarrow}$		$0.12^{\times 2\rightarrow}$							**0.84**	*1.00*
Cl2	0.11 0.09	0.13	0.12 0.08	0.09 0.11	0.12							**0.85**	*1.00*
Cl3	0.13	0.15 0.06	0.06	0.19 0.07	0.12 0.07							**0.85**	*1.00*
Sum	**2.00**	**1.94**	**1.88**	**1.91**	**1.95**	**1.87**	**1.91**	**1.86**	**1.81**	**0.38**	**3.96**		
Theor.	*2.00*	*2.00*	*2.00*	*2.00*	*2.00*	*2.00*	*2.00*	*2.00*	*2.00*	*0.26*	*4.50*		

Notes: Bond-valence values were calculated using the parameters of Krivovichev (2012) for Pb^{2+}–O bonds, Brese and O'Keeffe (1991) for Pb^{2+}–Cl bonds and Gagné and Hawthorne (2015) for the other bonds. *Calculated on the basis of chemical data.

This is the peer-reviewed, final accepted version for American Mineralogist, published by the Mineralogical Society of America.
The published version is subject to change. Cite as Authors (Year) Title. American Mineralogist, in press.
DOI: https://doi.org/10.2138/am-2024-9414. http://www.minsocam.org/

Table 4. Quantitative fit parameters for EXAFS analysis for As and Mo K-edge

Edge	**R factor**	**S_0^2**	**path**	**N**	**R (Å)**	**σ^2 (Å^2)**
Mo K-edge	0.014	0.9(1)	Mo-O	4	1.88(1)	0.006(1)
			Mo-O	1	1.75(1)	0.006(1)
			Mo-Pb	2	3.50(2)	0.003(3)
			Mo-Pb	2	3.59(3)	0.003(3)
			Mo-Pb	1	3.78(3)	0.003(3)
			Mo-Pb	2	3.9(2)	0.02(3)
			Mo-Pb	4	4.1(2)	0.02(3)
			Mo-Pb	1	4.2(2)	0.02(3)
			Mo-Cl	1	4.2(1)	0.001(11)
As K-edge	0.026	1.0(1)	As-O	4	1.69(1)	0.002(1)

Notes: Errors in brackets as reported by Artemis; S_0^2= Amplitude reduction factor; R = refined path distance; N=path degeneracy; σ^2= Debye-Waller factor (in order to reduce the total number of variables σ^2 parameter were refined as follows: one parameter for Mo-O paths, two parameters for Mo-Pb paths, split into two groups according to Mo-Pb distance, one parameter for Mo-Cl).

420

This is the peer-reviewed, final accepted version for American Mineralogist, published by the Mineralogical Society of America.
The published version is subject to change. Cite as Authors (Year) Title. American Mineralogist, in press.
DOI: https://doi.org/10.2138/am-2024-9414. http://www.minsocam.org/

421 Figure 1

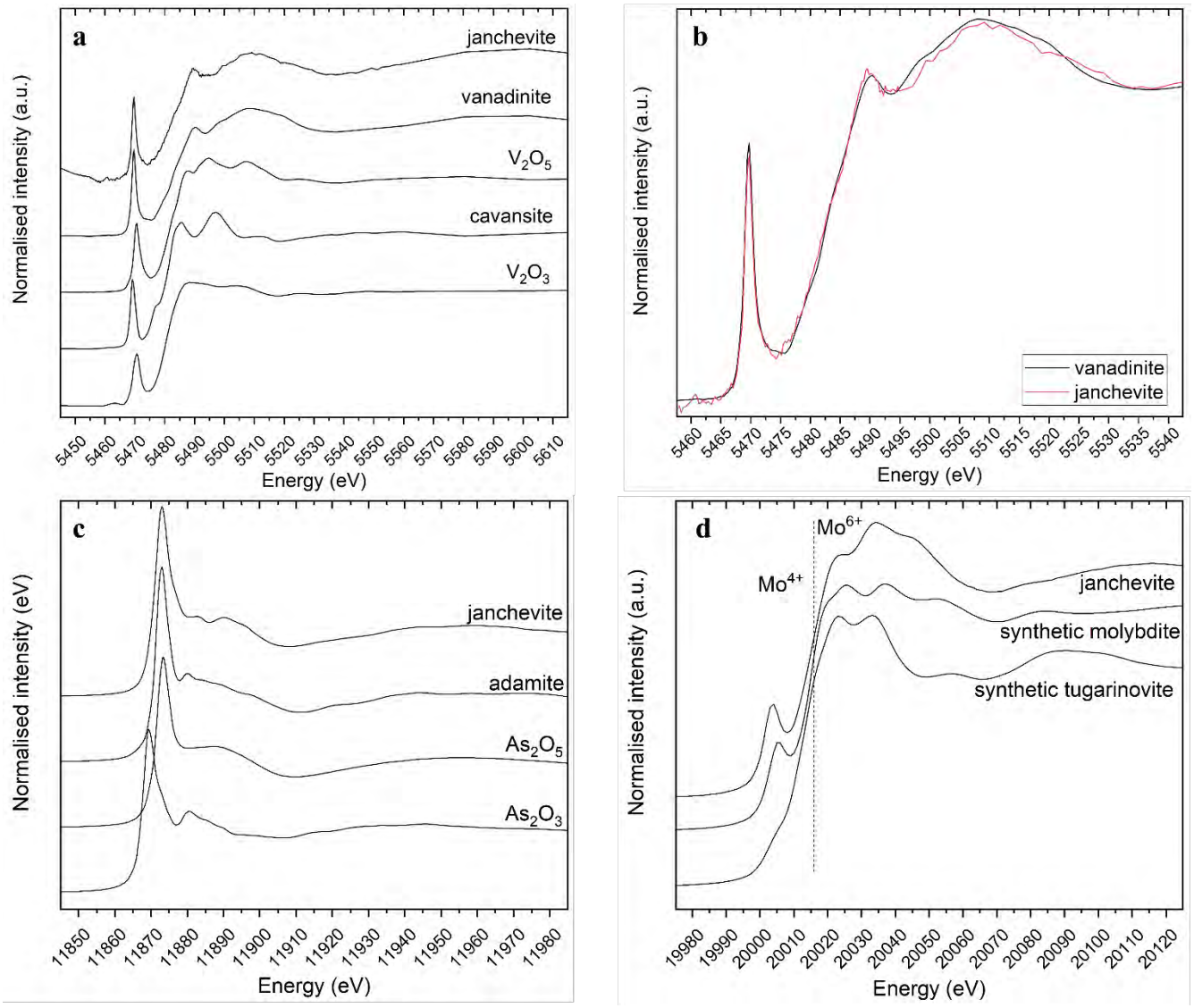

422

423

424

425

426

427

This is the peer-reviewed, final accepted version for American Mineralogist, published by the Mineralogical Society of America.
The published version is subject to change. Cite as Authors (Year) Title. American Mineralogist, in press.
DOI: https://doi.org/10.2138/am-2024-9414. http://www.minsocam.org/

428 Figure 2

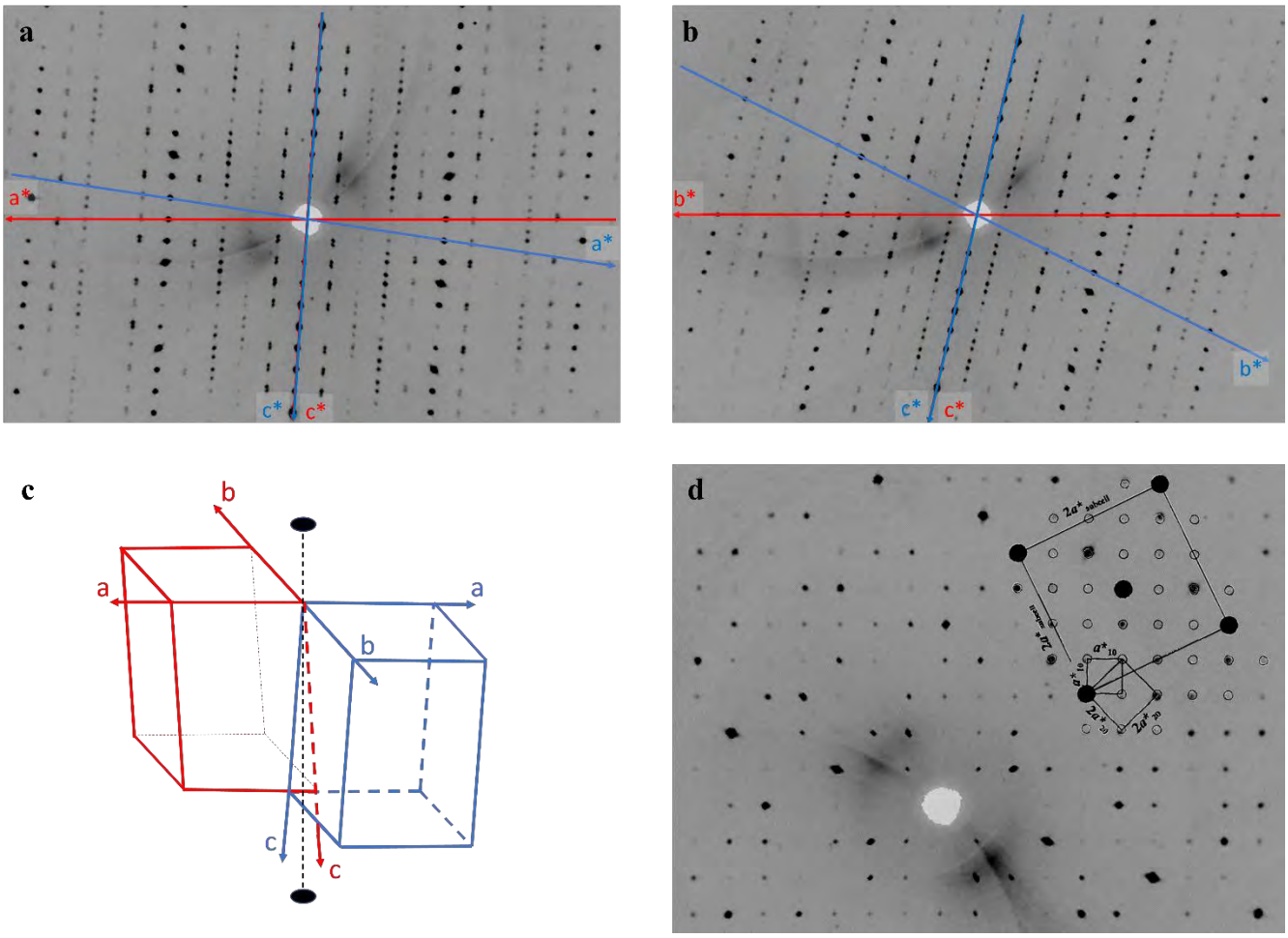

429

430

431

432

433

434

435

436

This is the peer-reviewed, final accepted version for American Mineralogist, published by the Mineralogical Society of America.
The published version is subject to change. Cite as Authors (Year) Title. American Mineralogist, in press.
DOI: https://doi.org/10.2138/am-2024-9414. http://www.minsocam.org/

437 Figure 3

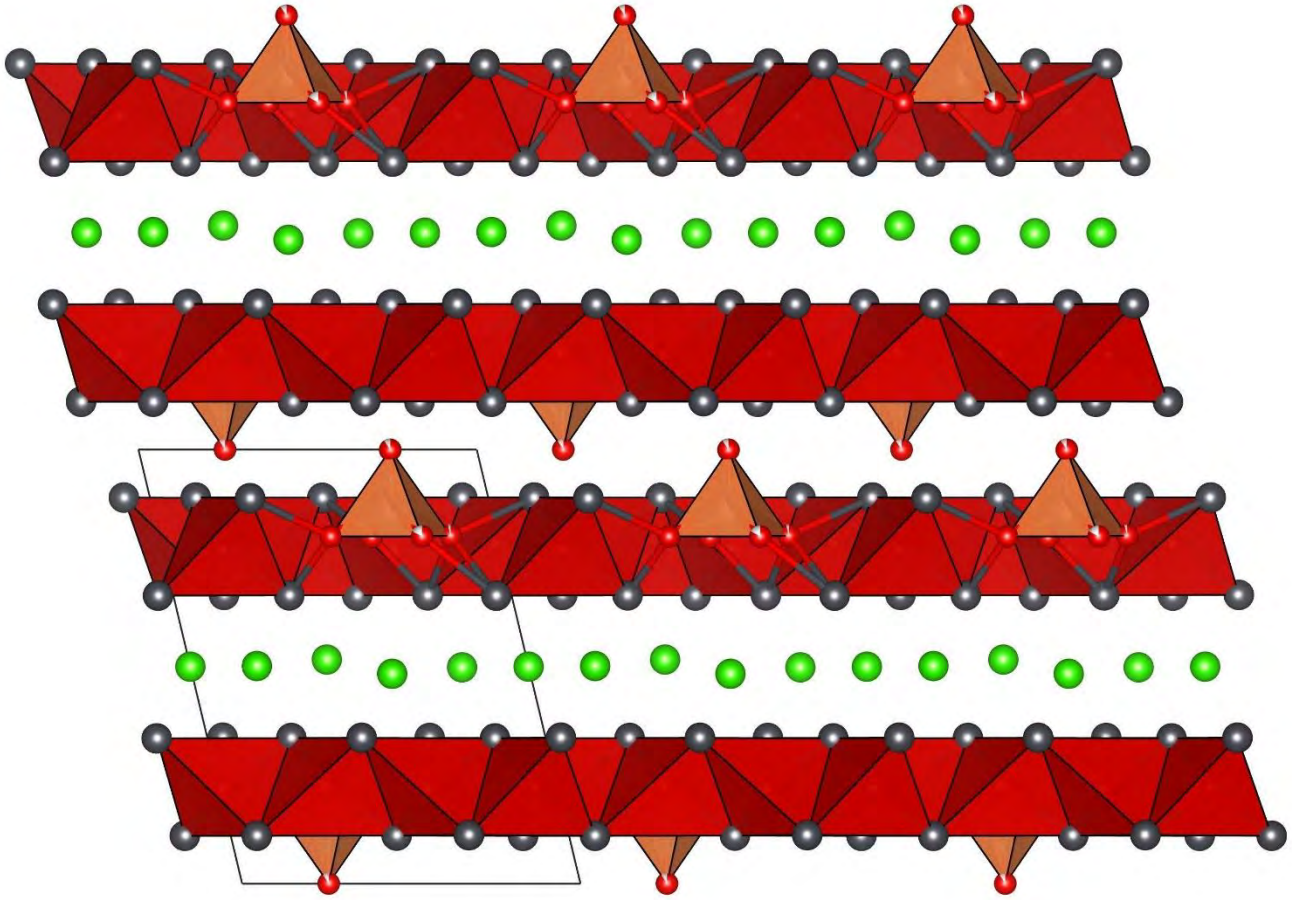

438

439

440

441

442

443

444

445

This is the peer-reviewed, final accepted version for American Mineralogist, published by the Mineralogical Society of America.
The published version is subject to change. Cite as Authors (Year) Title. American Mineralogist, in press.
DOI: https://doi.org/10.2138/am-2024-9414. http://www.minsocam.org/

446 Figure 4

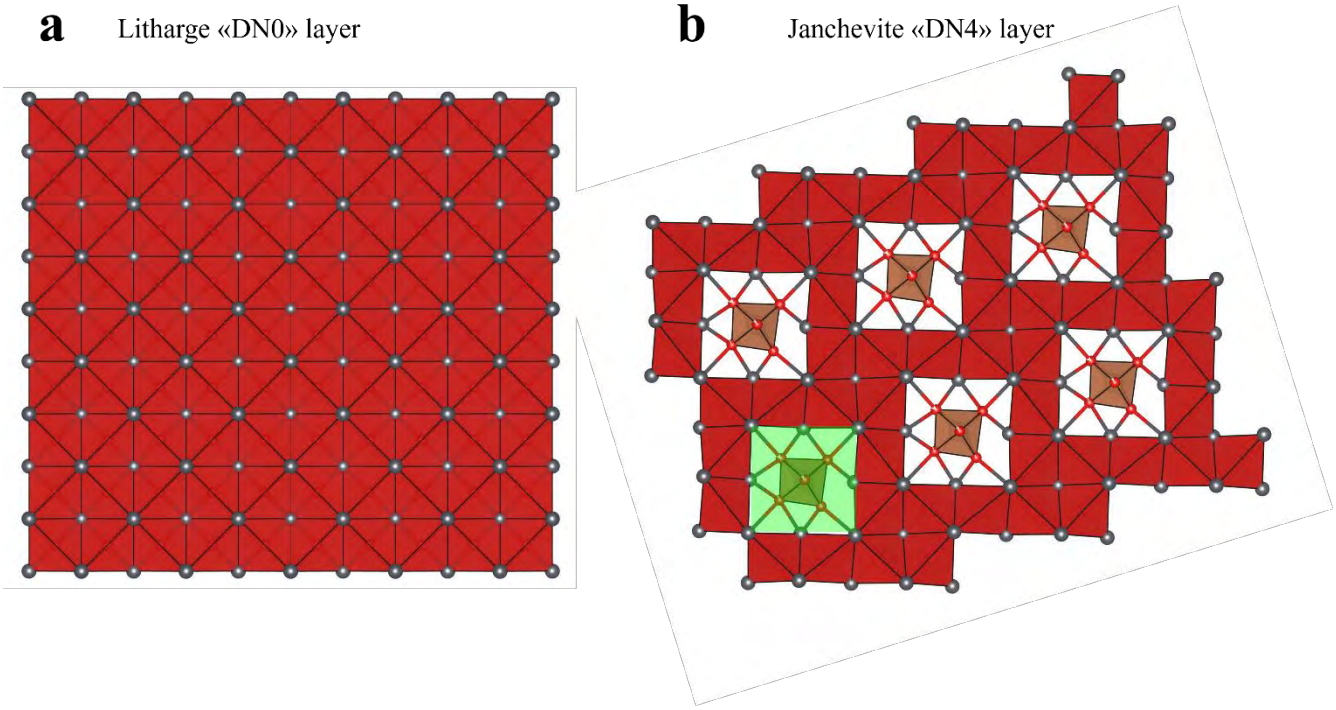

447

448

449 Figure 5

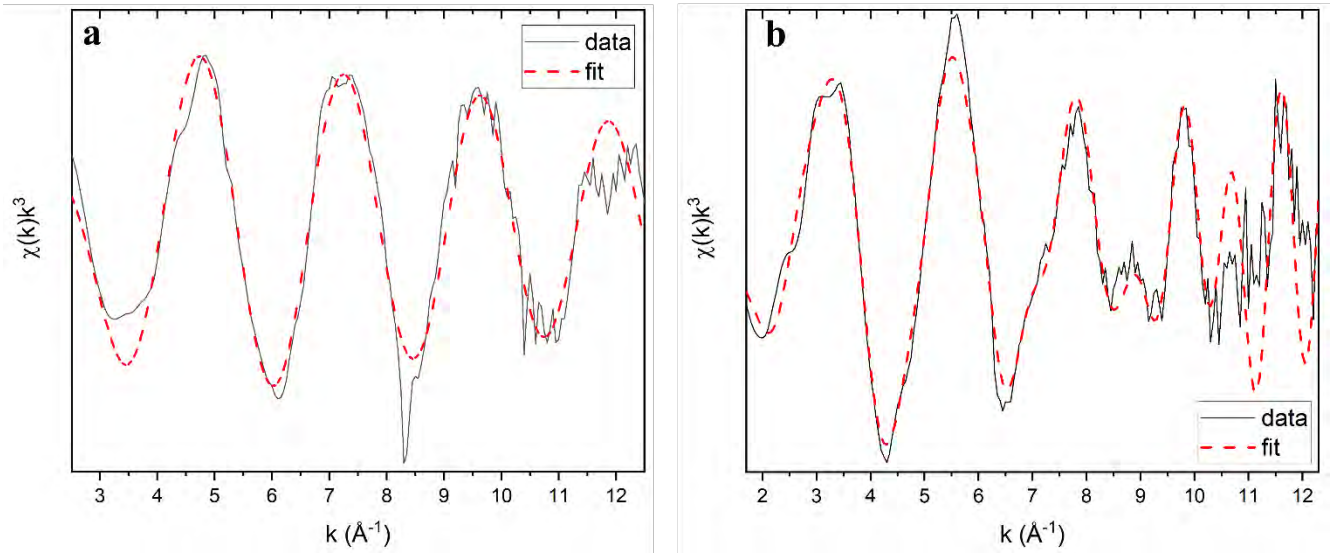

450

451

This is the peer-reviewed, final accepted version for American Mineralogist, published by the Mineralogical Society of America.
The published version is subject to change. Cite as Authors (Year) Title. American Mineralogist, in press.
DOI: https://doi.org/10.2138/am-2024-9414. http://www.minsocam.org/

452 Figure 6

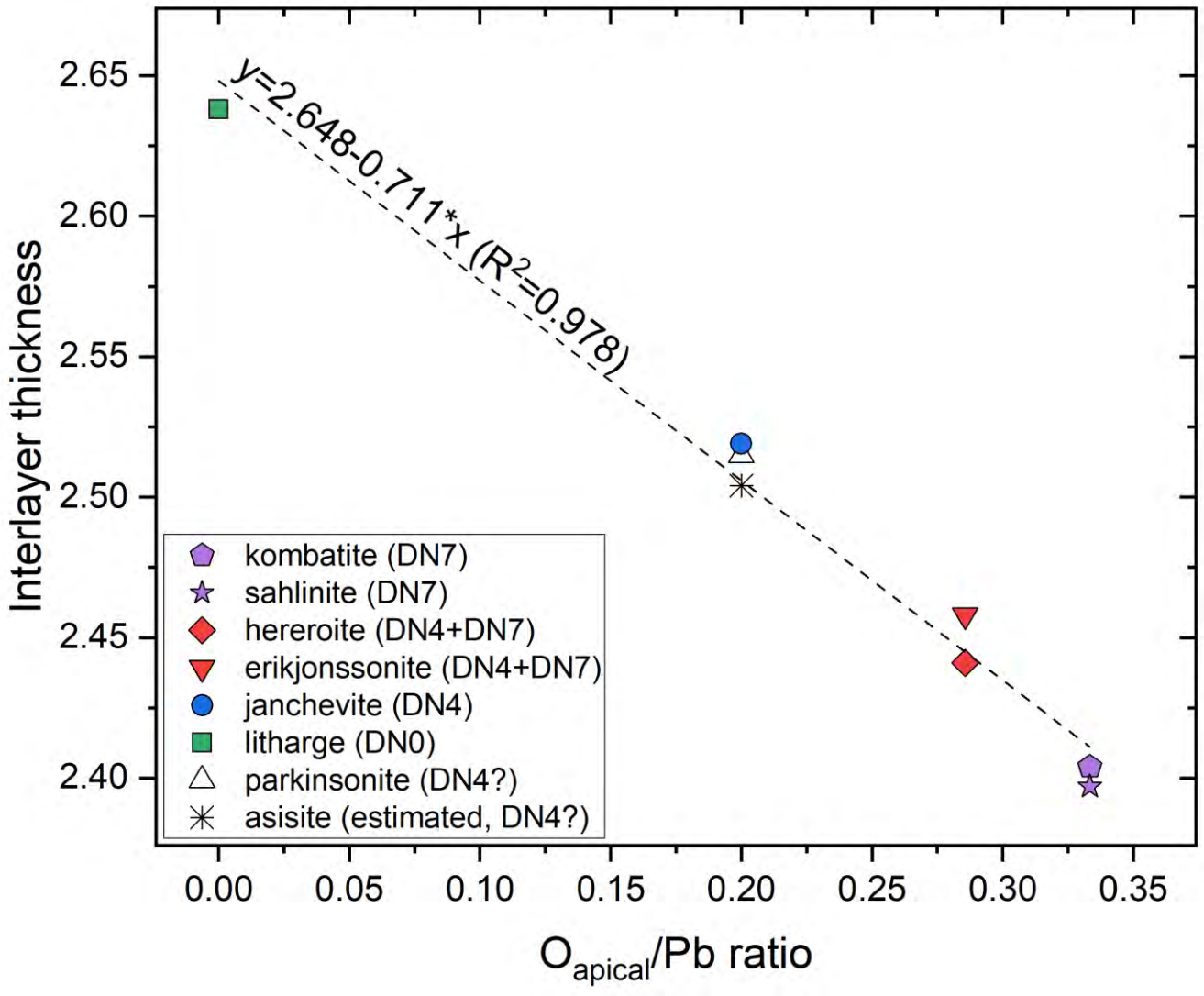

453

454